

Citation for published version:

Giardina, G, DeJong, MJ, Chalmers, B, Ormond, B & Mair, RJ 2018, 'A comparison of current analytical methods for predicting soil-structure interaction due to tunnelling', *Tunnelling and Underground Space Technology*, vol. 79, pp. 319-335. <https://doi.org/10.1016/j.tust.2018.04.013>

DOI:

[10.1016/j.tust.2018.04.013](https://doi.org/10.1016/j.tust.2018.04.013)

Publication date:

2018

Document Version

Peer reviewed version

[Link to publication](#)

Publisher Rights

CC BY-NC-ND

University of Bath

Alternative formats

If you require this document in an alternative format, please contact:
openaccess@bath.ac.uk

General rights

Copyright and moral rights for the publications made accessible in the public portal are retained by the authors and/or other copyright owners and it is a condition of accessing publications that users recognise and abide by the legal requirements associated with these rights.

Take down policy

If you believe that this document breaches copyright please contact us providing details, and we will remove access to the work immediately and investigate your claim.

A comparison of current analytical methods for predicting soil-structure interaction due to tunnelling

Giorgia Giardina^{*1}, Matthew J. DeJong², Benjamin Chalmers², Bryan Ormond², Robert J. Mair²

Abstract

Current procedures for the assessment of buildings response to tunnelling take into account the effect of soil-structure interaction through the definition of the building stiffness relative to the soil stiffness. Limitations of these procedures are uncertainties in the evaluation of structural parameters and inconsistent results between different methods. In this paper, three existing formulations of the Relative Stiffness Method (RSM) were been critically evaluated by analysing the governing factors in the building stiffness calculation and their effect on the structural damage assessment. The results of a sensitivity study on building height, eccentricity, opening ratio, tunnel depth, soil and masonry stiffness, and trough width parameter quantified the effect of these factors on the considered RSMs. The application of different RSMs to a real masonry building adjacent to the Jubilee Line tunnel excavation highlighted the significant effect of window openings, façade stiffness and neutral axis position on the building stiffness calculation and deformation prediction. These results highlight the need for a consistent and robust damage assessment procedure.

Keywords: building damage, building stiffness, masonry structures, relative stiffness, soil settlements, soil-structure interaction

1. Introduction

Underground constructions in urban areas require monitoring and protection of surface buildings. For large scale projects, like the North-South Line in Amsterdam, the Jubilee Line Extension and Crossrail in London, the costs connected to the preliminary damage assessment of structures can represent a large portion of the total project investment [1]. Damage prediction procedures are required to screen a large number of buildings in a relatively short time frame; furthermore, they need to be conservative, but accurate enough to avoid unnecessary further analyses.

Current methods applied to large projects involve a phased procedure where analyses of increasing complexity are applied to progressively smaller groups of buildings [2]. While offering the significant advantage of a rapid and extensive assessment, such a procedure has the limitation of not taking into account potentially relevant components

^{*}Corresponding author

Email address: g.giardina@bath.ac.uk (Giorgia Giardina^{*})

¹Department of Architecture and Civil Engineering, University of Bath, Claverton Down, BA2 7AY Bath, UK

²Department of Engineering, University of Cambridge, Trumpington Street, CB2 1PZ Cambridge, UK

16 of the building response until the very final phase. In particular, it neglects the interaction between the building and
17 the excavation-induced settlement trough when predicting the deformations of the soil-structure system.

18 More detailed methods exist which take this interaction into account [3–6]. These methods are based on the as-
19 sumption that the main component affecting the soil-structure interaction is the relative stiffness between the building
20 and the soil. However, these methods are not widely adopted in practice, due to concerns about the uncertainties in the
21 base assumptions and their effects on the final damage prediction. Major issues involve the calculation of the global
22 stiffness of the building under assessment, and disagreement regarding how to normalise the building stiffness with
23 the soil stiffness to produce a relative stiffness.

24 An important step towards the definition of a more robust damage assessment procedure consists of a better
25 understanding of the uncertainties and discrepancies in the available methods. This paper critically analyses the
26 existing relative stiffness methods for the assessment of excavation-induced damage to buildings. In particular, it
27 focuses on the evaluation of the global building stiffness, by investigating (a) what are the governing structural features
28 influencing the building stiffness calculation and (b) how uncertainties and assumptions in the definition of these
29 factors affect the final damage assessment.

30 In the following sections, a detailed summary of the available methods for the assessment of settlement-induced
31 damage is first presented, with a specific focus on procedures for calculating both the absolute and relative building
32 stiffness. A sensitivity study is then presented to broadly highlight the effect of buildings stiffness assumptions on the
33 final damage assessment. Subsequently, a case study is considered to more specifically quantify the effect of various
34 assumptions on damage assessment. Finally, the conclusions identify reasons for inconsistencies between the current
35 procedures and suggest opportunities towards the formulation of an improved method.

36 2. Literature review

37 2.1. Limiting Tensile Strain Methods (LTSM)

38 2.1.1. Bending-based strain criterion

39 This empirical-analytical method for the assessment of structural damage due to ground deformations was origi-
40 nally formulated by Burland et al. [7] and further developed by Boscardin and Cording [8]. First, the soil movements
41 due to the underground excavation are calculated without taking into account any interaction with adjacent structures.
42 These so-called greenfield displacements are then imposed to a simplified beam model of the building. Based on
43 Timoshenko beam theory [9], the maximum bending strain $\varepsilon_{b,\max}$ and the maximum diagonal strain $\varepsilon_{d,\max}$ are derived
44 as:

$$45 \varepsilon_{b,\max} = \frac{\Delta/L}{\left(\frac{L}{12t} + \frac{3I}{2tLH} \frac{E}{G}\right)} \quad (1) \quad \varepsilon_{d,\max} = \frac{\Delta/L}{\left(1 + \frac{HL^2}{18I} \frac{G}{E}\right)} \quad (2)$$

46 where L , H , I , E and G are the length, height, second moment of area of the building cross-section, the Young's and
47 the shear modulus of the equivalent beam, respectively, and t is the distance between the neutral axis and the edge

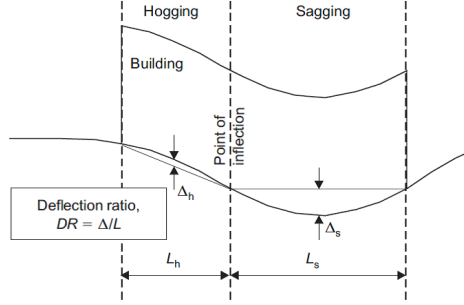


Figure 1: Deflection ratio for the sagging and hogging portions of the tunnelling-induced settlement trough [5].

48 of the beam in tension. Burland and Wroth [10] suggested an E/G value of 2.6 for masonry structures, assuming
 49 an isotropic elastic material with a Poisson's ratio of 0.3 for the equivalent beam. When applying the method to
 50 more flexible frame structures, they recommended a value of $E/G = 12.5$, although this method was later found to
 51 be unsuitable to capture the strain distribution [11]. Even for masonry structures, an effective E/G ratio is typically
 52 difficult to estimate, as it can be significantly affected by building dimensions and window openings, yet it strongly
 53 affects the calculation of the maximum bending and shear strains.

54 When predicting damage using the LTSM, differential vertical displacement is quantified by the deflection ratio
 55 Δ/L . As illustrated in Figure 1, Δ/L , and therefore the building strain, are calculated separately for the convex
 56 (sagging) and concave (hogging) portions of the settlement profile. Field data [12] has shown that buildings are
 57 generally more vulnerable to hogging than sagging deformations, mostly because in sagging the foundation offers an
 58 additional restraint to the settlement-induced deformation. For this reason, in Equations 1 and 2 the neutral axis is
 59 assumed to be in the middle of the beam in the sagging case ($t = H/2$) and at the lower beam edge in the hogging case
 60 ($t = H$) [10].

61 The beam horizontal strains are calculated as $\varepsilon_h = \delta/L$, where δ is the difference between the horizontal displace-
 62 ments of the greenfield profile at the two ends of the beam. The bending, diagonal and horizontal strains are then
 63 combined to obtain the total bending ε_{bt} and shear ε_{dt} strains:

$$64 \quad \varepsilon_{bt} = \varepsilon_{b,\max} + \varepsilon_h \quad (3) \quad \varepsilon_{dt} = \frac{\varepsilon_h}{2} + \sqrt{\left(\frac{\varepsilon_h}{2}\right)^2 + \varepsilon_{d,\max}^2} \quad (4)$$

65 The larger of these two values is the total strain of the structure, which is compared to limit values to determine the
 66 damage class for the structure (Table 1).

67 2.1.2. Shear-based damage criterion

68 Son and Cording [4] developed a similar approach, focusing on the shear component of the building deformation.
 69 According to Boscardin and Cording [8], they measured the deformations of building units (generally delimited by
 70 transversal bearing walls for masonry structures or columns for concrete frames) in terms of the following deformation

Table 1: Damage classification system [7, 8, 13].

Category of damage	Damage class	Description of typical damage and ease of repair	Approximate crack width (mm)	Limiting tensile strain levels (%)
Aesthetic damage	Negligible	Hairline cracks of less than about 0.1 mm width.	up to 0.1 mm	0 - 0.05
	Very slight	Fine cracks which can easily be treated during normal decoration. Perhaps isolated slight fracturing in building. Cracks in external brickwork visible on close inspection.	up to 1 mm	0.05 – 0.075
	Slight	Cracks easily filled. Redecoration probably required. Several slight fractures showing inside of building. Cracks are visible externally and some repainting may be required externally to ensure water tightness. Doors and windows may stick slightly.	up to 5 mm	0.075 – 0.15
Functional damage, affecting serviceability	Moderate	The cracks require some opening up and can be patched by a mason. Recurrent cracks can be masked by suitable linings. Repainting of external brickwork and possibly a small amount of brickwork to be replaced. Doors and windows sticking. Service pipes may fracture. Weather-tightness often impaired.	5 to 15 mm or a number of cracks > 3 mm	0.15 – 0.3
	Severe	Extensive repair work involving breaking out and replacing sections of walls, especially over doors and windows. Windows and door frames distorted, floors sloping noticeably. Walls leaning or bulging noticeably, some loss of bearing in beams. Service pipes disrupted.	15 to 25 mm, but also depends on number of cracks	> 0.3
Structural damage, affecting stability	Very severe	This requires a major repair involving partial or complete rebuilding. Beams loose bearing, walls lean badly and require shoring. Windows broken with distortion. Danger of instability.	usually > 25 mm, but depends on number of cracks	> 0.3

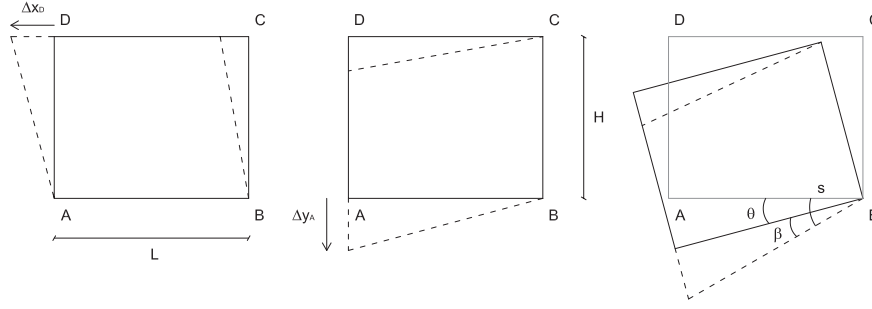


Figure 2: Deformation indicators (after Son and Cording [4]).

Table 2: Damage classification system [4].

Damage level	Damage	Critical tensile strain ε_c ($\times 10^{-3}$)
1	Negligible	0 – 0.5
2	Very slight	0.5 – 0.75
3	Slight	0.75 – 1.67
4	Moderate to severe	1.67 – 3.33
5	Severe to very severe	> 3.33

71 indicators (see Fig. 2): top horizontal strain $\varepsilon_{L,top} = \frac{\Delta x_D - \Delta x_C}{L}$, base horizontal strain $\varepsilon_{L,base} = \frac{\Delta x_A - \Delta x_B}{L}$, slope
 72 $s = \frac{\Delta y_A - \Delta y_B}{L}$, tilt $\theta = \frac{\Delta x_C - \Delta x_B}{H}$ and angular distortion $\beta = s - \theta$.

73 The maximum principal strain ε_p is calculated from the angular distortion β and the lateral strain ε_L : $\varepsilon_p =$
 74 $\varepsilon_L \cos(\theta_{max}^2) + \beta \sin(\theta_{max}) \cos(\theta_{max})$, where θ_{max} is the direction of crack formation and the angle of the plane in which
 75 ε_p acts, measured from the vertical plane: $\tan(2\theta_{max}) = \beta / \varepsilon_L$. The degree of damage is evaluated by comparing ε_p
 76 with defined values of critical tensile strain ε_c (Table 2).

77 2.2. Relative Stiffness Methods (RSMs)

Several researchers have proposed various procedures for extending LTSM methods to include soil-structure interaction by evaluating the relative stiffness of the building compared to the soil (Table 3). Potts and Addenbrooke [3] proposed a RSM that adjusts LTSM beam deflection using the following modification factors:

$$M^{DR,sag} = \frac{(\Delta_s/L_s)}{(\Delta_s/L_s)_{gr}} \quad M^{DR,hog} = \frac{(\Delta_h/L_h)}{(\Delta_h/L_h)_{gr}} \quad (5)$$

where Δ_s/L_s and Δ_h/L_h are the actual building deflection ratios, while $(\Delta_s/L_s)_{gr}$ and $(\Delta_h/L_h)_{gr}$ are the greenfield deflection ratios, i.e. the deflection ratios that would occur without the structure. Similarly, for the horizontal strains:

$$M^{\varepsilon_{hc}} = \frac{\varepsilon_{hc}}{\varepsilon_{hc}^{gr}} \quad M^{\varepsilon_{ht}} = \frac{\varepsilon_{ht}}{\varepsilon_{ht}^{gr}} \quad (6)$$

78 where ε_{hc} and ε_{ht} are the actual building horizontal strains in compression and tension, respectively, and ε_{hc}^{gr} and ε_{ht}^{gr}
 79 are the greenfield horizontal compressive and tensile strains. Potts and Addenbrooke [3] proposed design charts (Fig.

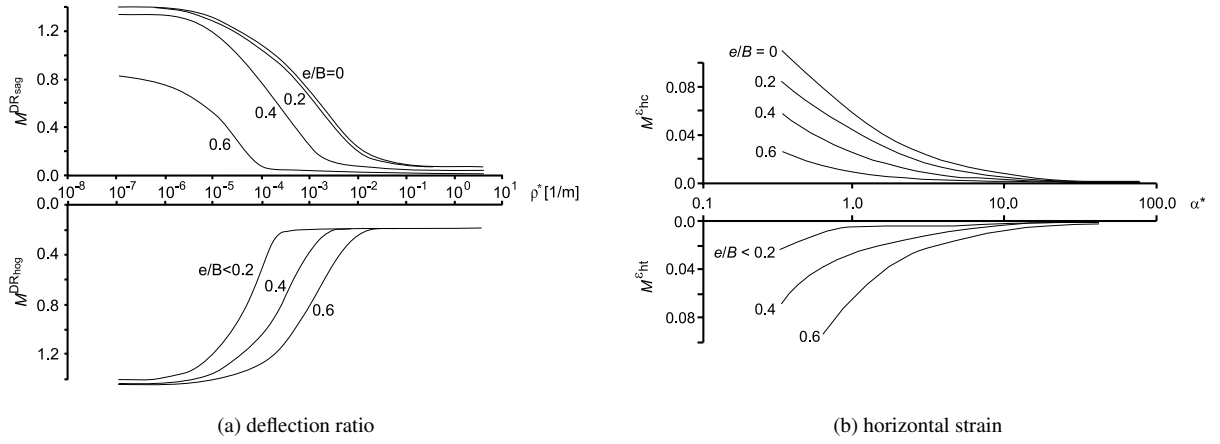


Figure 3: Design curves for modification factors [3]. Note that the dimension B corresponds to the building length L in the convention adopted in this paper.

3) to associate the modification factors to specific features of the building and the soil, summarised in the relative bending and axial stiffness:

$$\rho^* = \frac{EI}{E_s(L/2)^4} \quad (7) \quad \alpha^* = \frac{EA}{E_s(L/2)} \quad (8)$$

where A is the cross-section area, and E_s is the soil secant stiffness obtained at 0.01% axial strain in a triaxial compression test performed on a sample retrieved from a depth of $z_0/2$, where z_0 is the tunnel depth.

Franzius et al. [5] modified the relative stiffness, which was originally defined in plane strain conditions, to make it dimensionless in both two and three dimensions by including the effect of the tunnel depth and the building width B :

$$\rho_{mod}^* = \frac{EI}{E_s L^2 z_0 B} \quad (9)$$

$$\alpha_{mod}^* = \frac{EA}{E_s B L} \quad (10)$$

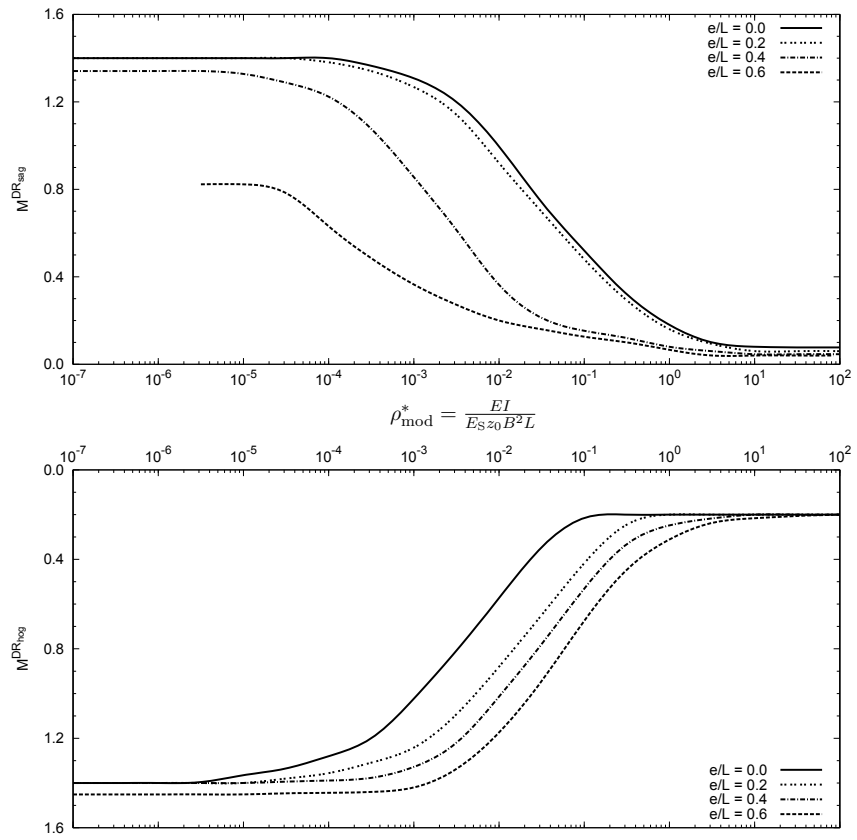
The design charts as modified by Franzius et al. [5] are shown in Figure 4.

Based on experimental tests and field data, Goh and Mair [6] partitioned the relative bending stiffness in the sagging and hogging zone of the greenfield settlement profile curvature (updated design charts are shown in Figure 5):

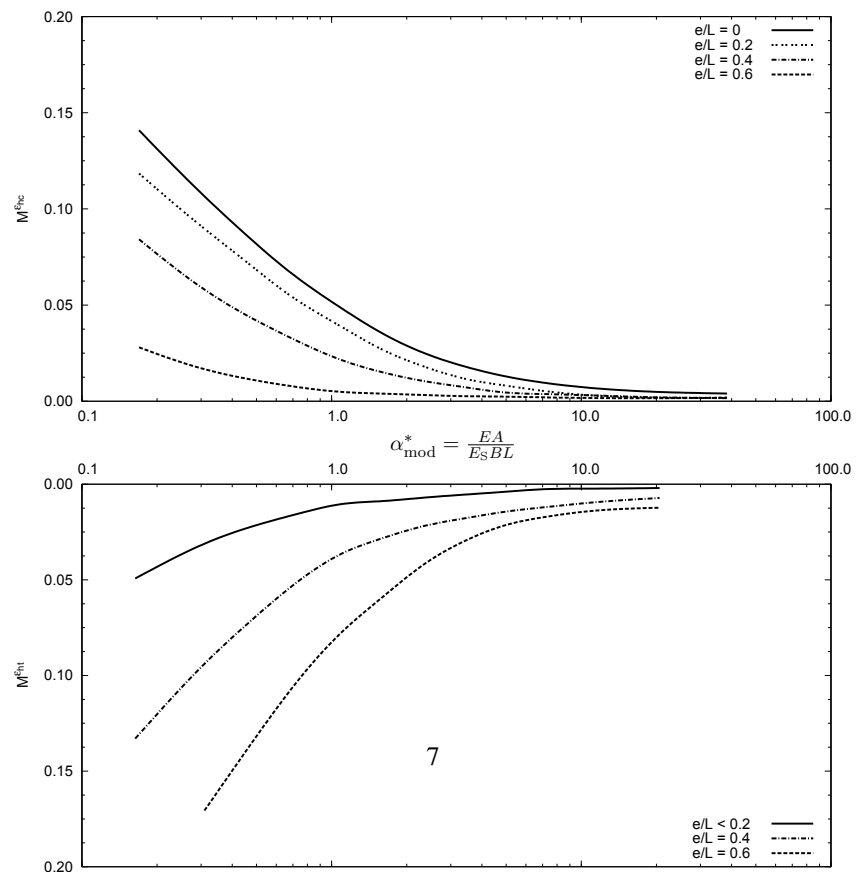
$$\rho_{sag,par}^* = \frac{EI}{E_s L_s^3 B} \quad \rho_{hog,par}^* = \frac{EI}{E_s L_h^3 B} \quad (11)$$

$$\alpha_{par}^* = \frac{EA}{E_s L} \quad (12)$$

Meanwhile, Son and Cording [4] took a notably different approach and proposed an RSM focused on the role of building shear stiffness in the soil-structure interaction; they developed an alternative definition of relative soil-building stiffness: $\frac{E_s L^2}{G H b_w}$, where E_s is the soil stiffness in the region of footing influence, G is the building elastic



(a) deflection ratio



(b) horizontal strain

Figure 4: Design curves for modification factors [5].

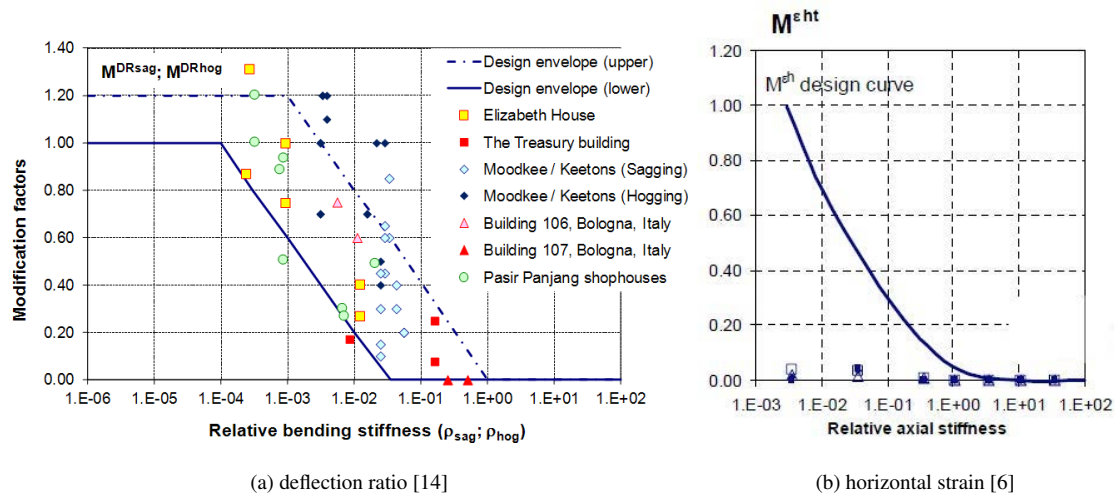


Figure 5: Design curves for modification factors.

89 shear modulus and b_w is the building wall thickness. Similarly to Potts and Addenbrooke [3], Son and Cording [4]
 90 developed a relationship between the relative stiffness and the building-induced reduction of greenfield deformation,
 91 though they quantified the deformation using the angular distortion β .

Table 3: Summary of main advantages and disadvantages of rapid methods for the assessment of settlement-induced damage to structures.

Method	Reference publication	Pros	Cons
Limiting Tensile Strain	Burland et al. [7], Boscardin and Cording [8], Burland et al. [13]	Rapid Easy to define geometrical input	Very conservative Difficult to define stiffness input No soil-structure interaction No opening effect
Relative stiffness	Potts and Addenbrooke [3], Son and Cording [4], Franzius et al. [5], Goh and Mair [6]	Soil-structure interaction	Difficult to define stiffness input

92 2.3. Calculation of building stiffness

93 One of the most difficult tasks in the application of the relative stiffness method is the determination of the overall
 94 bending stiffness of the building. An accurate calculation would require a detailed knowledge of the structural type,
 95 materials, construction techniques and current conditions; this information can be missing or not easily accessible at
 96 the time of the assessment. The task is made even more complicated by the need to select the most suitable calculation
 97 method among several proposed by different authors.

In their original formulation of the relative stiffness method, Potts and Addenbrooke [3] referred to two possible methods for the calculation of the building bending stiffness. For the method they predominantly used in their

analyses:

$$EI = E \sum_{i=1}^{n+1} (I_{\text{slab},i} + A_{\text{slab},i} d_i^2) \quad (13)$$

where i is the number of floor slabs, $I_{\text{slab},i}$ is the second moment of area of each slab, $A_{\text{slab},i}$ is the cross-sectional area of each slab, n is the number of storeys, d_i is the vertical distance between the structure's neutral axis and the slab's neutral axis. Since this formula can overestimate the stiffness of framed structures, they suggested the following alternative:

$$EI = E \sum_{i=1}^{n+1} (I_{\text{slab},i}) \quad (14)$$

where the shear transfer between the slabs is ignored, and the total building stiffness simply results from the sum of the bending stiffness of each slab. In both cases the axial stiffness EA is the sum of the axial stiffness values for each slab:

$$EA = E \sum_{i=1}^{n+1} (A_{\text{slab},i}) \quad (15)$$

98 The alternative approach suggested in Eq. 14 is based on the formula proposed by Meyerhof [15] for a multi-
 99 storey building frame: $EI = E \sum_{i=1}^n (I_i)$, where n is the number of storeys and I_i is the second moment of area of a single
 100 storey: $EI_i = EI_b \left[1 + \left(\frac{K_l + K_u}{K_b + K_l + K_u} \right) \frac{L^2}{l^2} \right]$. In the previous equation, $K_b = I_b/l_b$ is the average stiffness of beams,
 101 $K_l = I_l/h_l$ is the average stiffness of lower columns, $K_u = I_u/h_u$ is the average stiffness of upper columns, L is the
 102 building length, l_b is the beam length, $h = (h_l + h_u)/2$ is the average storey height.

103 Meyerhof [15] also included estimations for different building typologies. For multi-storey building frame with
 104 in-filled panels $EI = \sum_{i=1}^n \left[EI_i + \frac{(EI)_p L^2}{2h^2} \right]$, where $(EI)_p$ is the bending stiffness of the panel in the vertical plane, while
 105 for load bearing walls without openings where b_w is the average thickness of the wall and H is the height of the wall
 106 or the structure $EI = \frac{Eb_w H^3}{12}$.

Melis and Rodriguez Ortiz [16] developed an unified approach for different structural typologies:

$$EI = \sum (EI)_{\text{floors}} + \sum (EI)_{\text{walls}} + \sum (EI)_{\text{basements}} \quad (16)$$

107 where $(EI)_{\text{floors}} = E \left(\frac{1}{12} Bb_s^3 + Bb_s d^2 \right) \frac{1}{B}$ is the contribution of each floor slab, $(EI)_{\text{walls}} = E \left(\frac{1}{12} b_w H^3 + b_w H d^2 \right) \frac{1}{B}$ is
 108 the contribution of each wall, $(EI)_{\text{basements}} = E \left(\frac{1}{12} Bb_b^3 + Bb_b d^2 \right) \frac{1}{B}$ is the contribution of each foundation slab rigidly
 109 connected to the superstructure and $(EI)_{\text{basements}} = E \left(\frac{1}{12} Bb_b^3 + Bb_b c^2 \right) \frac{1}{B}$ is the contribution of each foundation slab
 110 in case of basement hinged to the superstructure.

111 In these equations, b_s and b_b are the slab and basement thickness, respectively, d is the distance from the slab to
 112 the neutral axis of the structure, assumed at the mid-height of the structure, and c is the distance from the assumed
 113 hinge between the superstructure and the basement. The second moment of area of walls, continuous footings and/or
 114 foundation slabs forming the basement are calculated relative to the neutral axis of the basement. The second moment
 115 of area of each slab relative to its own middle plane is typically neglected, as well as the stiffness of columns in

Table 4: Reduction factor on building bending stiffness EI due to openings [16].

Type of wall	Length $< 2H$	Length $> 2H$
No openings	1.00	1.00
Openings from 0 to 15%	0.70	0.90
Openings from 15 to 25%	0.40	0.60
Openings from 25 to 40%	0.10	0.15

116 conventional frame structures. Partition walls are also neglected, due to their reduced stiffness; in case of internal
 117 bearing walls, they can be included as external walls. A novelty in the approach by Melis and Rodriguez Ortiz [16]
 118 was the inclusion of reduction factors to consider the effect of door and window openings. The reduction factors are
 119 dependent on the percentage of openings and the aspect ratio of the structure (Table 4).

120 In the numerical study that led to the formulation of Equations 9 and 10, Franzius et al. [5] considered only
 121 concrete frames. By assuming the neutral axis at the mid-length of the building they calculated the bending and axial
 122 stiffness according to Eq. 13 and 15, respectively. Mair and Taylor [17] evaluated the building stiffness of historic
 123 buildings adjacent to the Jubilee Line Extension as $EI = E \frac{bH^3}{12}$, where b is the unit building width.

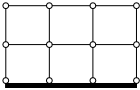
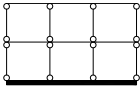
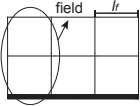
124 Dimmock and Mair [18] later modified the calculation of the bending stiffness for masonry structures on shallow
 125 strip foundations in the hogging zone by neglecting the wall contribution: $EI = E \frac{bh_f^3}{12}$, where h_f is the height of the
 126 foundation, and not the entire height of the masonry wall. Furthermore, in the sagging zone, they proposed a 90%
 127 reduction in the masonry wall stiffness.

The equivalent tensile strains calculated with the LTSM (Eqs. 1 and 2) for massive walls are conceptually incon-
 sistent if applied to frame structures. Furthermore, the effect of the modified E/G factor on the tensile strain depends
 on the L/H ratio of the building and not representative for all kinds of frame structures. Therefore, Netzel [11] pre-
 sented a new approach to evaluate the influence of the imposed settlements on the beams and columns of a frame
 structure. The maximum bending moment M_{\max} and shear force V_{\max} of the fictitious beam are calculated as:

$$M_{\max} = \frac{\Delta}{L} \frac{12EI}{L} \quad V_{\max} = \frac{\Delta}{L} \frac{24EI}{L^2} \quad (17)$$

128 For the calculation of the equivalent second moment of area, three types of frame structures are considered, de-
 129 pending on the structural connections between floor and columns (Table 5). The maximum value of bending moment
 130 and shear force calculated with Equations 17 are redistributed to the structural elements, considering the different
 131 distribution of stiffness in the three frame typologies (Table 5). The structure is then verified for the increased values
 132 of bending moments and shear forces.

Table 5: Calculation of equivalent second moment of area and additional bending moment and shear force for frame structures [11].

Frame type	I equivalent	Additional M and V
Hinged connections between beams and columns	$I = I_b$	$M_b = \frac{I_b}{I} M_{\max}$ $V_b = \frac{A_b}{A} V_{\max}$
	where I_b is the second moment of area of the continuous foundation plate	where M_b and V_b are the additional moment and shear force concentrated in the foundation plate, respectively, and A_b is the cross-sectional area of the foundation plate
Hinged connections between columns or walls and continuous beams	$I = I_b + \sum_{i=1}^n I_{s,i}$	$M_b = \frac{I_b}{I} M_{\max}$ $V_b = \frac{A_b}{A} V_{\max}$ $M_{s,i} = \frac{I_{s,i}}{I} M_{\max}$ $V_{s,i} = \frac{A_{s,i}}{A} V_{\max}$
	where I_s is the second moment of area of one floor slab	where $M_{s,i}$ and $V_{s,i}$ are the additional moment and shear force concentrated in each floor slab, respectively, and $A_{s,i}$ is the cross-sectional area of one floor slab
Full monolith connections between beams and columns	$I = I_b + \sum_{i=1}^n \left[I_{s,i} \left(1 + \frac{1}{\frac{I_{s,i}/l_{f,i}}{I_{u,i}/h_{u,i} + I_{l,i}/h_{l,i}} + 1}} n_f^2 \right) \right]$	A numerical analysis is required to evaluate the redistribution of the moment and the shear forces to the individual structural elements
	where n_f is the amount of fields, $l_{f,i}$ is the length of one field, $I_{u,i}$ and $I_{l,i}$ are the second moment of area of column/wall above and below considered floor slab, and $h_{u,i}$ and $h_{l,i}$ are the storey height above and below the considered floor slab, respectively	

133 3. Sensitivity study

134 To quantify the effects of the assumptions described in the previous section, this section presents a parametric
135 analysis performed on a number of building models with different structural features. The LTSM [7] and three RSMs
136 [3, 5, 6] were applied.

137 3.1. Tunnelling-induced settlements

Tunnelling-induced greenfield settlements were calculated according to Peck [19]:

$$S_v(x) = S_{v,\max} e^{-\frac{x^2}{2i^2}} \quad (18)$$

where $S_{v,\max}$ is the maximum settlement measured above the tunnel axis, x is the horizontal distance from the tunnel axis and i is the horizontal distance between the tunnel axis and the point of inflection of the settlement trough. By defining the volume loss percentage V_L as a function of the volume of ground lost V_S per meter of tunnel and the diameter D : $V_L = \frac{V_S}{\pi D^2}$. $S_{v,\max}$ can be derived as $V_L = \frac{0.313V_L D^2}{i}$, where $i = kz_0$, k is the trough width parameter and z_0 is the tunnel depth. The horizontal component S_h of the ground displacement were calculated according to O'Reilly and New [20]:

$$S_h(x) = -\frac{x S_v(x)}{z_0} \quad (19)$$

138 The 1 mm cut-off and the splitting at the inflection point of the settlement trough, as proposed by Mair et al. [2],
139 were applied.

140 3.2. Damage classification

141 The deflection ratio and average horizontal strain were used to calculate the limiting tensile strain for each structure
142 (Section 2.1). For all structures it was assumed that $E/G = 2.6$. The bending stiffness of each structure was calculated
143 according to Melis and Rodriguez Ortiz [16] (Eq. 16) by assuming that the global neutral axis was at the mid-height
144 of the structure. The same reduction depending on façade openings was applied to the axial stiffness. Equations 7,9
145 and 11 were used to calculate the relative stiffness for the three considered RSMs; the modification factors were then
146 derived from the corresponding design charts (Figs. 3, 4, 5). Based on these modification factors and on the greenfield
147 deformations (Section 3.1), the actual deflection ratio and horizontal strain of the building were calculated and used
148 to determine the total tensile strain.

149 3.3. Reference structure

150 The geometry of the reference case is illustrated in Figure 6. The structural features are based on a typical masonry
151 Georgian town house with strip foundations. The wooden floor beams were assumed to run perpendicularly to the
152 building direction and therefore to have negligible impact on the global stiffness of the structure. The tunnel has

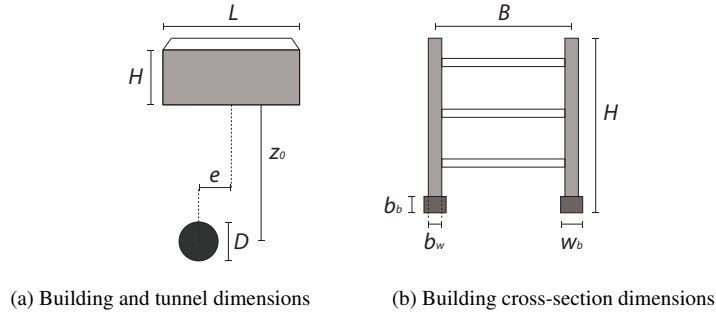


Figure 6: Reference structure geometry.

153 depth and diameter similar to the Crossrail tunnels and the soil parameters are the same as assumed by Potts and
 154 Addenbrooke [3]. Table 6 reports the dimensions and parameters of the reference model. Figure 7 compares the
 155 relative stiffness and modification factor values for the reference buildings calculated accordingly to the analysed
 156 RSMs. The envelope defined by Goh and Mair [6] is shown for reference.

Table 6: Sensitivity study: reference model parameters.

Component	Variable	Value
Building	Length L	25 m
	Height H	10 m
	Width B	10 m
Façade	Thickness b_w	0.25 m
	Stiffness E_w	3 GPa
	Openings ratio O	20%
Foundation	Thickness b_b	0.3 m
	Width w_b	0.4 m
	Stiffness E_b	3 GPa
Tunnel	Depth z_0	25 m
	Diameter D	7.18 m
	Volume loss V_L	1%
Soil	Trough width parameter k	0.5
	Reference stiffness E_s	124.5 MPa

157 3.4. Variable parameters

158 The sensitivity study aimed to investigate the effect of the following parameters on the field damage assessment:

- 159 • **Building height** By keeping constant the reference length L of the building and varying the building height H ,
 160 the influence of the L/H ratio and therefore the bending-shear strain decomposition on the damage assessment
 161 was evaluated. The selected range includes building from one to six storeys.

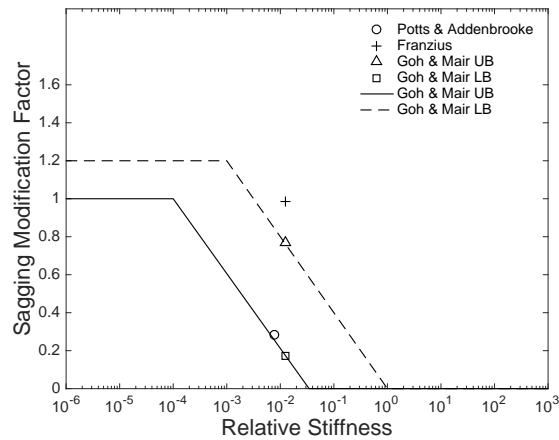


Figure 7: Relative stiffness and modification factor for the reference building: comparison between RSMs. Note that Potts & Addenbrooke's relative stiffness is given in [1/m], while the Franzius' and Goh & Mair's values are dimensionless.

- 162 • **Building eccentricity** Changing the building position with respect to the tunnel axis enabled assessment of the
163 effect of splitting the settlement profile into the sagging and hogging parts for the different damage assessment
164 methods.
- 165 • **Opening ratio** The influence of the building openings was quantified by varying the ratio between window
166 openings and total area of the façade. The selected range of variations spans from façades with no openings to
167 façades with half of their surface covered by windows.
- 168 • **Tunnel depth** The tunnel depth affects both the horizontal displacement through Equation 19 and the vertical
169 displacement through Equation 18, via the location of the point of inflection $i = kz_0$. The selected range of
170 tunnel depth corresponds to a minimum cover-to-diameter (C/D) ratio of 1.6 (shallow tunnel) to a maximum of
171 5 (deep tunnel).

172 Furthermore, the impact of potential errors in the estimation of the material parameters was taken into account
173 by varying the **soil stiffness**, **masonry stiffness** and **trough width parameter**. The variation range includes typical
174 values for historic masonry. The soil stiffness range includes typical values from granular material to clay. Similarly,
175 a large variety of soils from sand to clay have been considered for the trough width parameter. The ranges for all
176 assumed variations are listed in Table 7. Each parameter variation was performed for three different values of building
177 length (15, 25 and 35 m) and three volume losses (0.1, 0.15 and 0.2 %). A total number of 7128 configurations
178 was analysed. Each parameter variation was performed for three different values of tunnel depth (15, 25 and 40 m),
179 building height (5, 10 and 20 m), building length (15, 25 and 35 m), opening ratio (0, 20 and 50%) and volume
180 loss (0.1, 0.15 and 0.2 %). A total number of 192456 configurations were analysed. Sections 3.6.1 to 3.6.5 discuss
181 selected results which illustrate the most significant trends. When not specified as varying, the presented parameters
182 correspond to the reference values (Table 6).

Table 7: Sensitivity study: parametric ranges.

Variable	Lower limit	Upper limit
Building height H	5 m	20 m
Building length L	15 m	35 m
Building eccentricity e	-24.5 m	37.5 m
Openings ratio O	0%	50%
Volume loss V_L	1 %	2 %
Tunnel depth z_0	15 m	40 m
Masonry stiffness $E_m = E_w = E_b$	1 GPa	6 GPa
Soil ref. stiffness E_s	25 MPa	175 MPa
Trough width parameter k	0.2	0.7

183 3.5. Global sensitivity study

184 To quantify the overall sensitivity of the damage assessment outputs to the tunnel and building geometrical param-
 185 eters, and to the uncertainties in material parameters, a total effect sensitivity index [21] was calculated for each of the
 186 factors listed in Table 7. The use of a total sensitivity index allowed to evaluate the model sensitivity over the entire
 187 input parameter space and quantify the effect of each input parameter and its coupling with other input parameters.

Similarly to recent applications of global sensitivity analyses to geotechnical problems [22], the calculation of
 the total effect sensitivity index S_{Ti} was based on two independent (N, P) matrices \mathbf{A} and \mathbf{B} , each one containing N
 random samples of the input parameter vector $\mathbf{X} = X_1, X_2, \dots, X_P$, and P (N, P) matrices \mathbf{C}_i , each one equal to the matrix
 \mathbf{B} but with its i th column copied from \mathbf{A} . For each of the P parameters i , S_{Ti} was calculated as [22]:

$$S_{Ti} = \frac{(\mathbf{y}_B - \mathbf{y}_{Ci})^T (\mathbf{y}_B - \mathbf{y}_{Ci})}{2\mathbf{y}_B^T \mathbf{y}_B - 2N(\bar{\mathbf{y}}_B)^2} \quad (20)$$

188 where \mathbf{y}_B and \mathbf{y}_{Ci} are vectors containing the model evaluation for matrix \mathbf{B} and \mathbf{C}_i , respectively, while $\bar{\mathbf{y}}_B$ is the mean
 189 of the values contained in \mathbf{y}_B .

190 The (N, P) matrices \mathbf{A} and \mathbf{B} were randomly generated by using a uniform probability density function, within
 191 the ranges reported in Table 7, for $N=10,000$ samples and $P=9$ parameters. The corresponding sagging and hogging
 192 modification factors and the total strain values were used as model evaluation.

193 3.6. Results

194 The outcomes of the parametric study were compared in terms of influence of the considered parameters.

195 3.6.1. Building stiffness

196 Figures 8 and 9 show the effect of opening percentage, tunnel cover-to-diameter (C/D) ratio and building height-
 197 to-length (H/L) on the building bending and axial stiffness calculation. An increase in opening percentage has a
 198 significant influence in reducing the stiffness; the sharp drop in stiffness at 40% openings is due to the façade contri-
 199 bution being completely neglected when the openings are more than 40% of the total façade area [16]. The facade

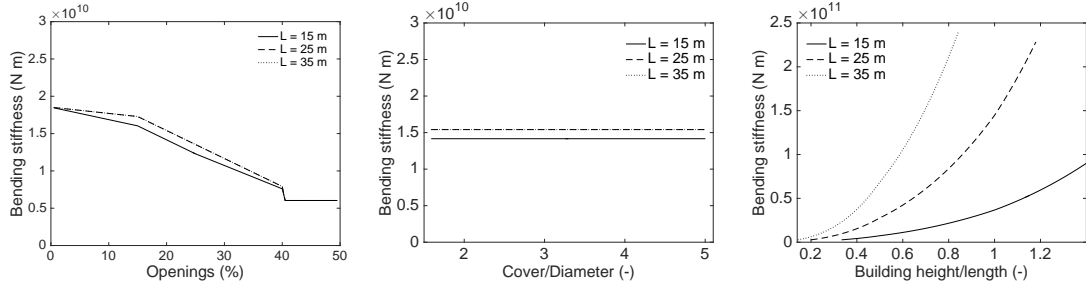


Figure 8: Sensitivity study: bending stiffness variation with openings, C/D and H/L ratio.

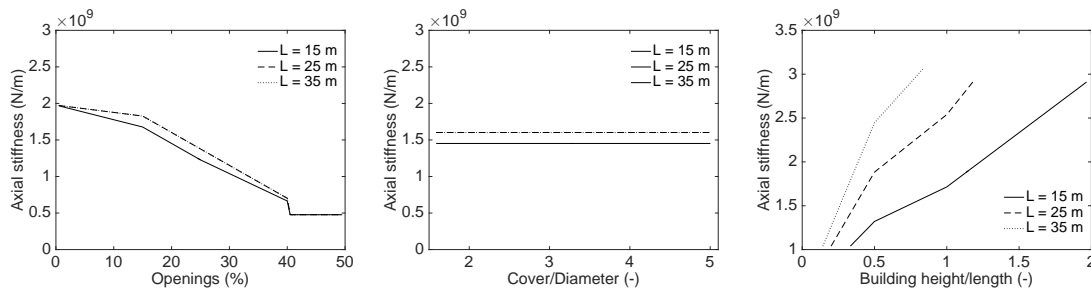


Figure 9: Sensitivity study: axial stiffness variation with openings, C/D and H/L ratio.

200 stiffness is proportional to H^3 , so it is expected that height has the largest effect on the building stiffness. The building
 201 axial stiffness is roughly proportional to H .

202 The tunnel depth does not play any role in the stiffness calculation. However, the plots including varying C/D
 203 ratio clearly show that the axial and bending stiffness are slightly dependent on L . Although L is not a parameter
 204 directly included in the stiffness formulation, the reduction factors [16] are dependent on the H/L ratio, as well as on
 205 the percentage of openings.

206 3.6.2. Building located symmetrically above tunnel (sagging case)

207 For a building located symmetrically above the tunnel (i.e., $e = 0$), three different building lengths were again
 208 considered and the parameters were varied. Note that for the variations in opening percentage and building H/L
 209 ratio, the inflection point of the greenfield settlement occurs at 12.5 m from the tunnel centerline, so the building is in
 210 sagging. For the variation of tunnel C/D ratio, the position of the inflection point varies from 7.5 to 40 m.

211 Figure 10 shows significant variability in the sagging modification factors predicted by the RSMs considered.
 212 These variations are due to the differing modification factor charts, but also due to the different methods of calculating
 213 the relative stiffness (Eqs. 7, 9, 11). In general, Franzius et al. [5] gave the most conservative assessment, while Potts
 214 and Addenbrooke [3] usually predicted a modification factor between the upper and lower bound estimations of Goh

215 and Mair [6]. All methods were affected by the building length, as expected based on the relative bending stiffness
 216 formulations.

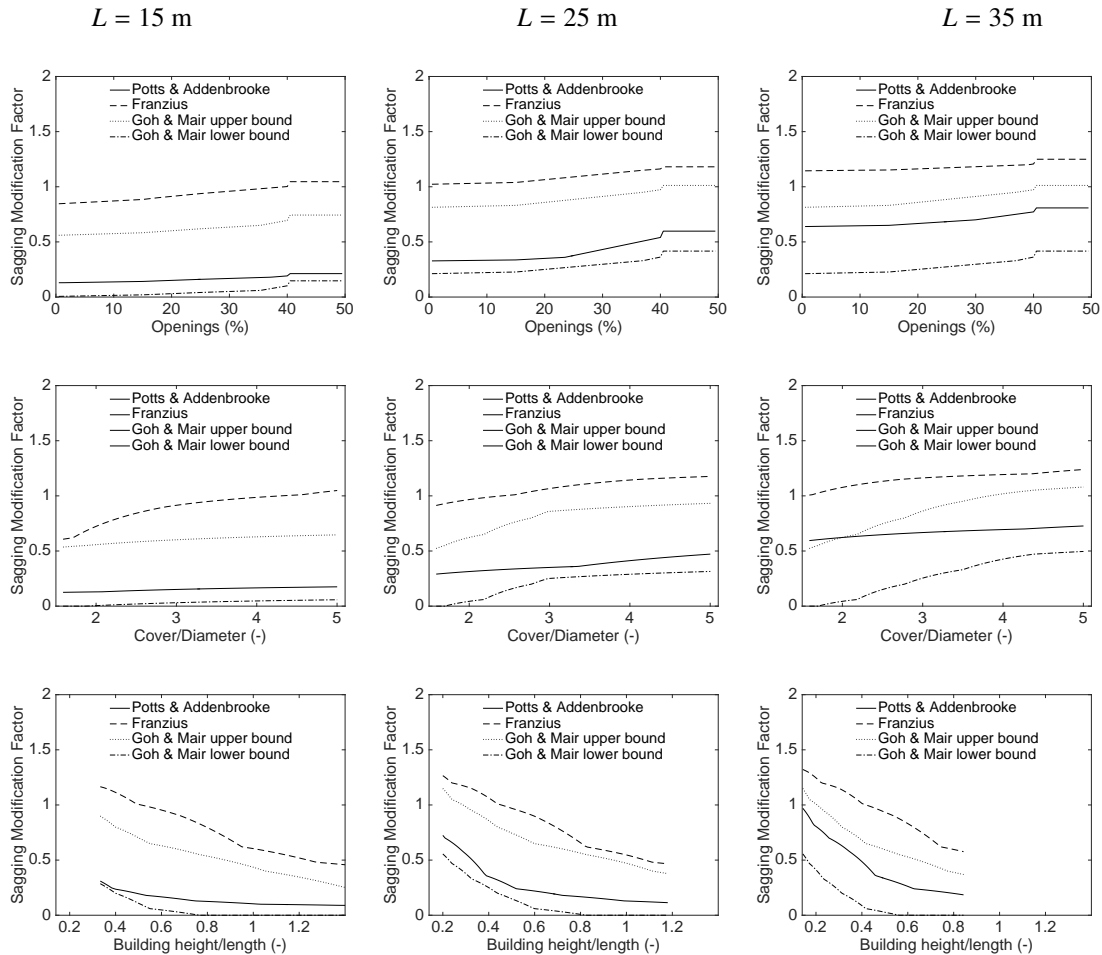


Figure 10: Sensitivity study results, sagging: variation of deflection ratio modification factors with openings, C/D and H/L ratio.

217 The trends in response to varying parameters were similar, although the sensitivity of the RSMs varied. For
 218 example, the Potts and Addenbrooke [3] formulation is less sensitive to tunnel depth than the other methods. The
 219 tunnel depth affects the relative stiffness both directly and indirectly. In all RSM formulations, the soil stiffness
 220 increases with tunnel depth, so the relative stiffness (Eqs. 7 to 12) decreases. This causes the building to deform more
 221 closely to the ground movements, increasing the modification factor. This trend is similar for all RSMs. However, in
 222 addition to this effect, Franzius et al. [5] directly included the tunnel depth in the relative bending stiffness (Eq. 9),
 223 and Goh & Mair's partitioning method causes a change in L_s with tunnel depth, causing a more sensitive response to
 224 tunnel depth. Numerous other effects of the RSM assumptions can be similarly evaluated using Figure 10.

225 The predicted horizontal strain modification factors are essentially zero for the range of parameters considered
226 in Figure 10 (plots not shown for brevity). Thus, the horizontal strain is negligible for almost all cases considered.
227 The only exception is the case where the stiffness of the façade is completely neglected because of an opening ratio
228 $> 40\%$, so the only contribution to the axial stiffness is given by the shallow foundation.

229 Figure 11 shows the predicted total tensile strain for 1% surface volume loss for the same variation of parameters
230 as in Figure 10. The total strains labelled greenfield were derived from the greenfield displacements and are dependent
231 on the tunnel properties and the external building geometries, as defined in Equations 1 to 4, but are independent of the
232 building stiffness and therefore the opening percentage. Only 1% volume loss results are included because that was the
233 typical volume loss used for Crossrail building damage predictions. Additional volume losses were also investigated,
234 but mostly show similar trends to Figure 11, with an increase in total tensile strain for higher volume losses. In
235 Figure 11, the significant reduction of strain predicted by all the RSMs is dominated by the fact that the horizontal
236 strain modification factor is approximately zero for nearly all cases considered. For many cases, the deflection ratio
237 modification factors alone would not predict such a drastic reduction.

238 For the sagging case, the variation of strain with the building height depends on the building length. This is due
239 to the combined effect of the H/L and Δ/L ratios on the bending and shear components of the strain (Eqs. 1 and 2).
240 This effect can be observed in the variation of the greenfield curve, which is decreasing with the building H/L ratio
241 for relatively small H/L values and increasing with H/L for larger H/L values. In the RSMs, the reduction in strain
242 with H/L is amplified by the dependence of the building stiffness on H^3 .

243 The variation of tunnel C/D ratio has the most significant impact on the total tensile strain. The tunnel depth
244 affects the relative stiffness both directly and indirectly, as indicated above. Furthermore, it influences the calculation
245 of the deflection ratio. A reduction in z_0 reduces the spacing of the inflection point $i = kz_0$; this results in an increased
246 curvature of the settlement profile, which is quantified by the increase in Δ/L . Depending on the building length, a
247 reduction in z_0 from 35 to 15 m can lead to an increase of the LTSM predicted strain larger than 100%. This factor is
248 particularly relevant near to stations, where it is convenient to construct the tunnels as close as possible to the surface,
249 to minimise the depth of station boxes and reduce the costs. In these areas, tunnels are shallower and construction
250 techniques generally result in greater volume losses; therefore, the LTSM is expected to predict a relatively high level
251 of potentially vulnerable buildings. When the RSMs are applied, the predicted strain decreases between 40% and 90%,
252 depending on the specific method and the building length.

253 3.6.3. *Building located in pure hogging region*

254 The same building model and variable ranges were used to analyse the pure hogging case. The eccentricity of the
255 structure is defined as $e = kz_0 + \frac{L}{2}$. Figure 12 shows the influence of opening ratio, tunnel C/D ratio and building H/L
256 ratio on the deflection ratio and horizontal strain modification factors, respectively. In this case, e is constant for the
257 variations of opening and H/L ratio, but since k is defined by the tunnel depth, e varies with C/D so that the structure

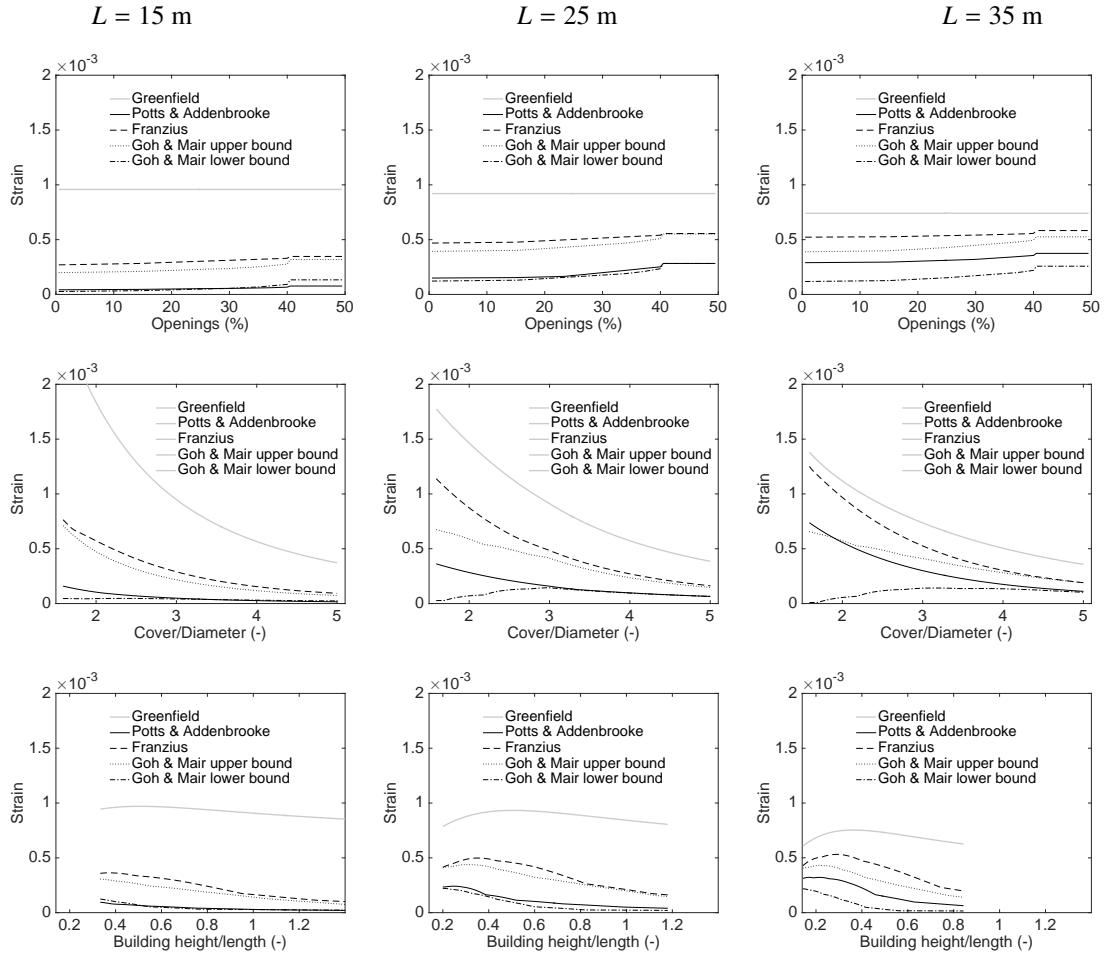


Figure 11: Sensitivity study results, sagging: total strain variation with openings, C/D and H/L ratio, $V_L = 1\%$

258 is always subjected to the pure hogging profile which exhibits the maximum differential settlement along the building
 259 length.

260 An increased relative eccentricity e/L needs to be considered when using the design charts by Potts and Adden-
 261 brooke [3] and Franzius et al. [5] (Figs. 3a and 4b). For each design chart, a 2D interpolation of the modification factor
 262 matrices was performed by using the relative stiffness and the relative eccentricity as reference values. The increased
 263 e/L ratio leads to higher modification factors for the corresponding variations of the relative stiffness method, even
 264 if the relative bending stiffness is the same as in the sagging case. Goh and Mair [6] use the same design charts but
 265 define different relative stiffness for the hogging and sagging case (Eq. 11).

266 Since L_h is defined by the location of the inflection point and the 1 mm cut off point (approximately at $2.5i$, where
 267 $i = kz_0$), a reduction in tunnel depth z_0 leads to a reduction in L_h . The effect of decreasing the length of the hogging
 268 zone is evident when C/D is smaller than 2.8.

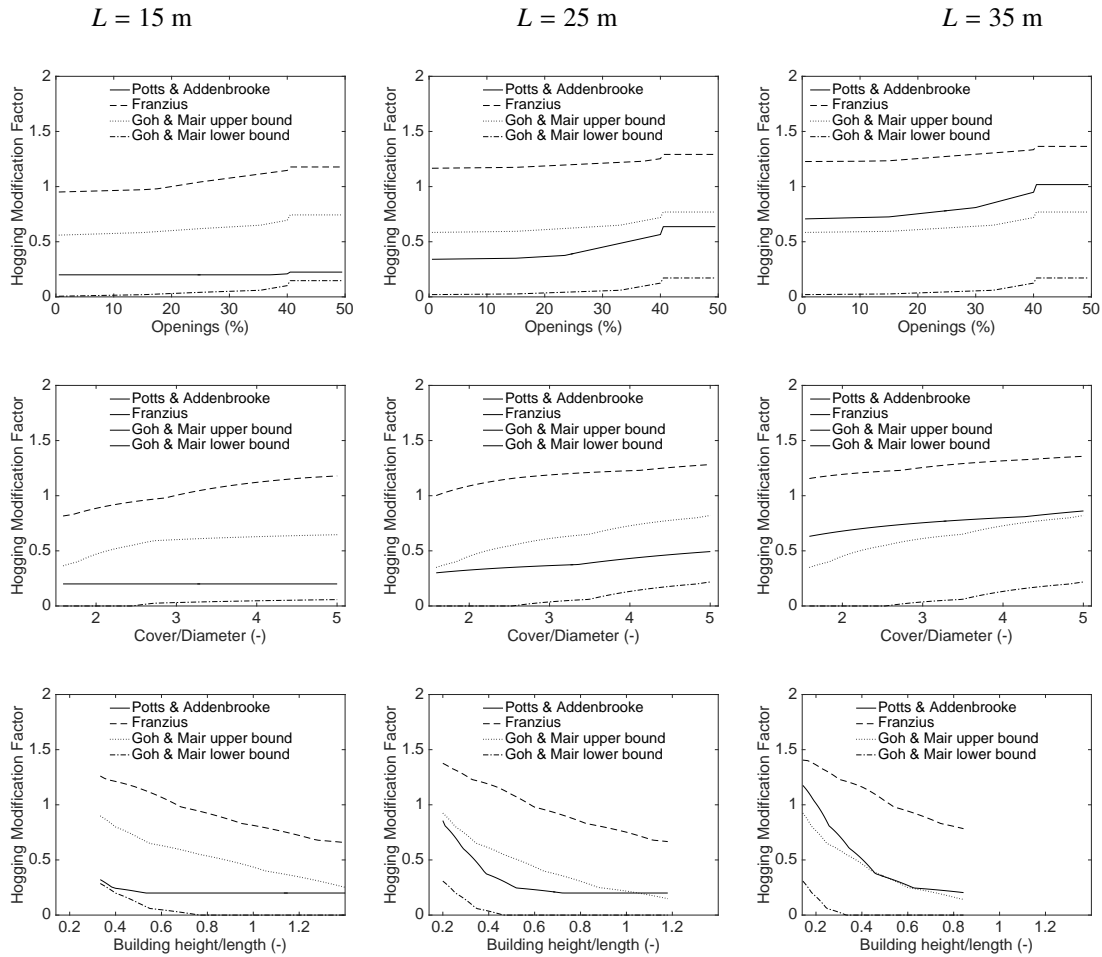


Figure 12: Sensitivity study results, hogging: variation of deflection ratio modification factors with openings, C/D and H/L ratio.

269 The hogging modification factors reported in Figure 12 show trends similar to the sagging modification factors
 270 (Fig. 10). Additionally, the Franzius RSM predicted the largest modification factor, while the Potts & Addenbrooke's
 271 assessment again tended to fall between the Goh & Mair upper and lower bound curves. However, for longer build-
 272 ings ($L=35$ m), the different weight of L_h in Goh & Mair's relative stiffness formulation (Eq. 11), combined with
 273 Goh & Mair's design charts (Fig. 5), caused the Goh & Mair upper and lower bounds to give the lowest hogging
 274 modification factors. The predicted horizontal strain modification factors are again essentially zero, apart from when
 275 opening percentages are greater than 40%.

276

277 The differences observed between sagging and hogging modification factors propagate to the strain calculation.
 278 Figure 13 shows the strain prediction for a structure in pure hogging at 1% volume loss. Due to the reduced deflection
 279 ratio of the greenfield settlement trough in the hogging zone, the predicted strain is lower in hogging than in sagging.
 280 The general variations with openings, C/D and H/L ratio are similar to the ones observed in the sagging case (Fig. 11),
 281 and the significant reduction in strain compared to the greenfield is again dominated by the horizontal modification
 282 factor being approximately zero.

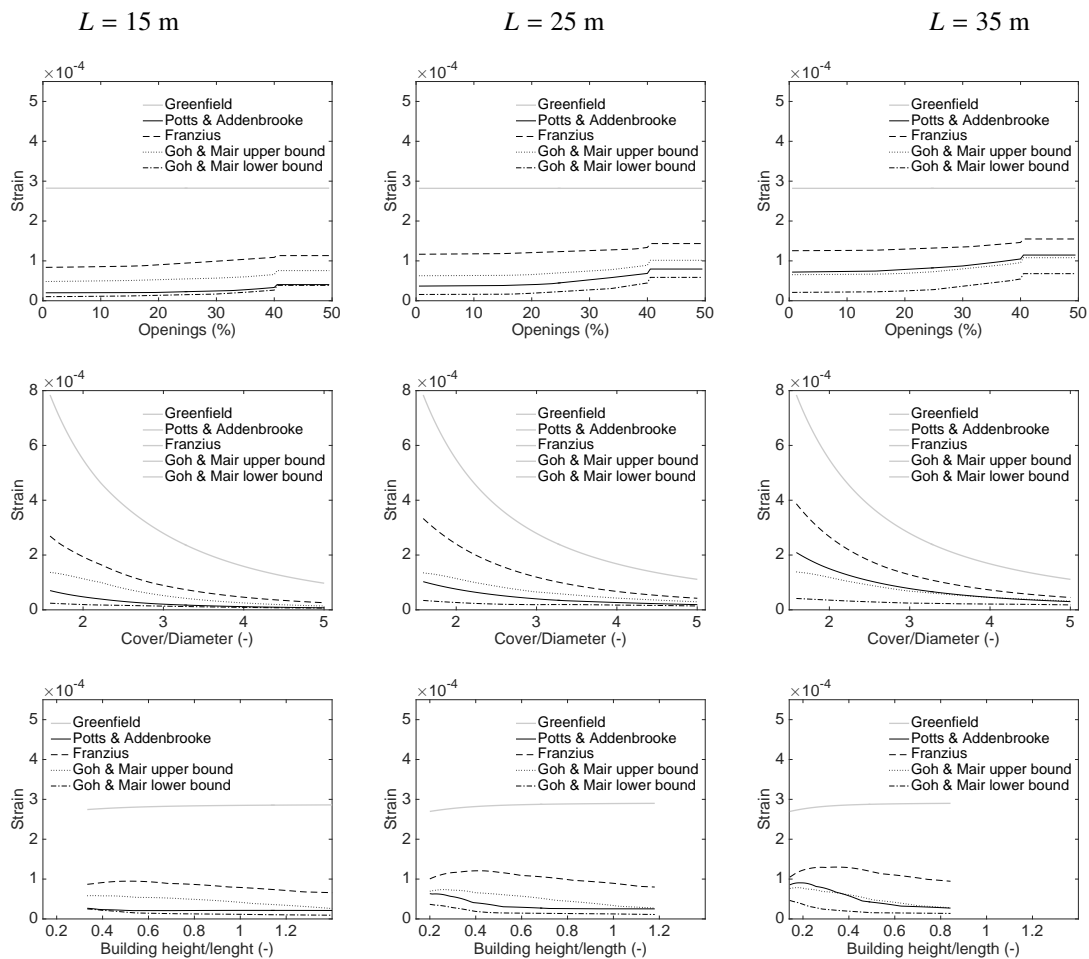


Figure 13: Sensitivity study results, hogging: total strain variation with openings, C/D and H/L ratio, $V_L = 1\%$.

283 3.6.4. Eccentricity

284 Sections 3.6.2 and 3.6.3 discuss buildings located primarily in hogging or sagging, while this section considers a
 285 smooth variation of building position. Potts and Addenbrooke [3] and Franzius et al. [5] design curves vary with the
 286 relative eccentricity e/L ; higher relative eccentricities result in smaller modification factors for the sagging case and
 287 larger modification factors for the hogging case. Goh and Mair [6] design curves are independent from the building

288 eccentricity. In their formulation, e affects the final assessment through its influence on the sagging and hogging
289 building length: shorter L_s and L_h lead to smaller $\rho_{\text{sag,par}}^*$ and $\rho_{\text{hog,par}}^*$.

290 Figure 14 shows the variation of the modification factors and the total tensile strain as a function of the building
291 eccentricity over the trough width (e/i) ratio for increasing values of building length. A volume loss of 1% is con-
292 sidered. Potts and Addenbrooke [3] and Franzius et al. [5] modification factors directly reflect the different design
293 curve trends for the hogging and sagging case: sagging modification factors decrease and hogging modification fac-
294 tors increase with an increase in eccentricity. Similarly, Goh and Mair [6] modification factors directly depend on the
295 sagging and hogging relative stiffness definitions (Eq. 11).

296 For buildings centered near the inflection point, where the curvature of the settlement trough is minimum, the strain
297 decreases significantly for both the LTSM and RSM methods. Since the average curvature over a longer building is
298 always less than the maximum curvature at the tunnel axis, increasing the building length in the LTSM framework
299 results in a lower greenfield deflection ratio and therefore a lower maximum strain that occurs over a wider range of
300 eccentricities. Total strains are progressively larger for increasing volume losses, but the trends are similar (plots not
301 shown).

302 3.6.5. Uncertain material parameters

303 Several material parameters which are involved in the relative stiffness calculation are difficult to assess without
304 a significant amount of testing. Figure 15 quantify the effect of potential uncertainties in the trough width parameter
305 k , soil stiffness E_s and masonry stiffness E_m on the damage assessment. A 25 m long building located symmetrically
306 above the tunnel and a volume loss of 1% are considered.

307 The soil properties (k and E_s) have no effect on the bending and axial building stiffness. Assuming that both the
308 façade and foundation are masonry, the building bending and axial stiffness are proportional to the masonry stiffness.
309 The trough width parameter has no effect on the sagging modification factors for Potts and Addenbrooke [3] and
310 Franzius et al. [5], while it significantly affects the prediction by Goh and Mair [6]. Varying k influences the location
311 of the inflection point and therefore changes the maximum size of the sagging zone. In the presented case, when
312 $k > 0.5$ the structure is fully contained within the sagging zone of the greenfield settlement trough and therefore the
313 modification factor remains constant.

314 All the relative stiffness formulations are inversely proportional to the soil stiffness E_s . The considered range is
315 much larger than the typical variation for an individual project, as the extreme values here refer to soft Singapore
316 clay and very stiff London clay. Assuming a more realistic range of 50 MPa for an individual tunnelling project, the
317 modification factors can vary by 15%. All the modification factors decrease with the increase in masonry stiffness,
318 as expected. The horizontal modification factors are again essentially zero across the entire range of all parameters
319 considered (plot not shown), allowing the horizontal strain to be neglected, again provided that openings are less than
320 40%.

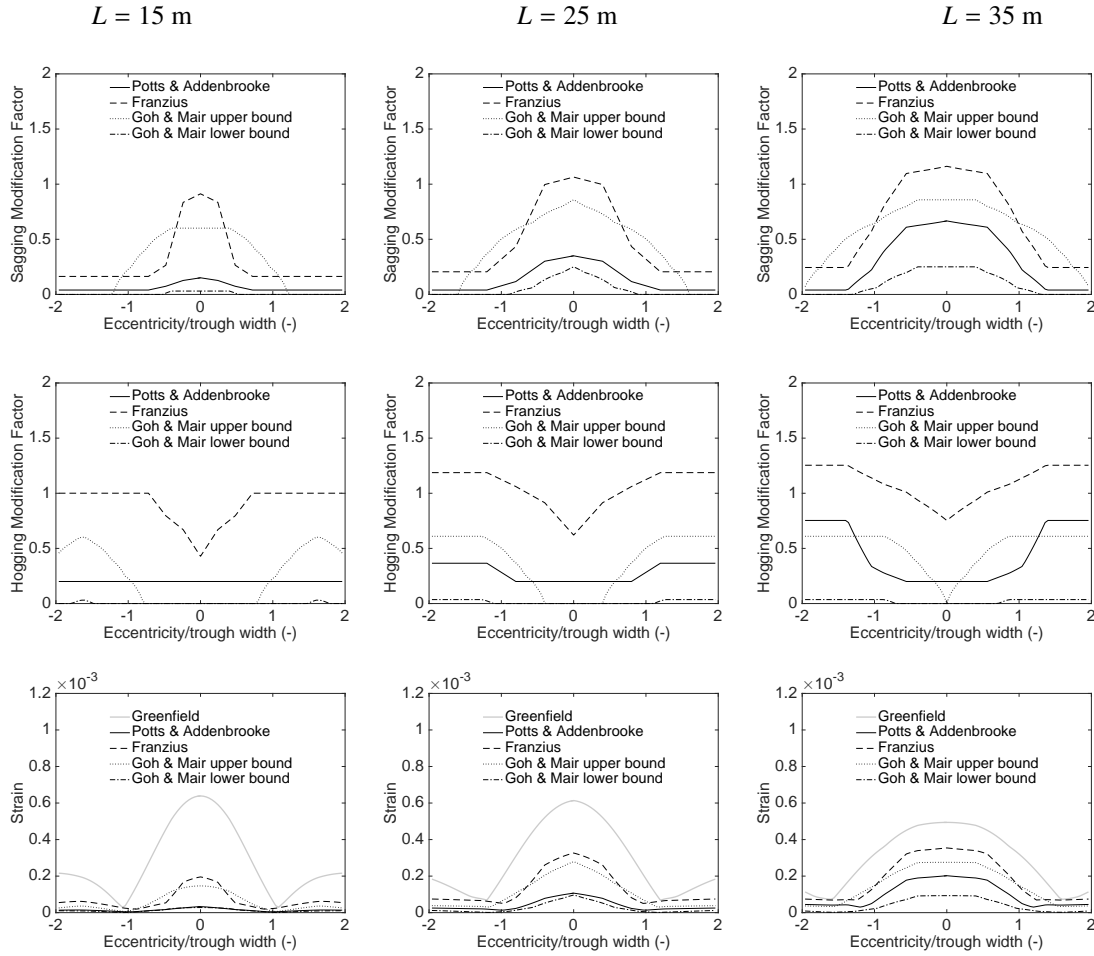


Figure 14: Sensitivity study results, total strain vs e/i ratio.

321 Assuming a constant E/G ratio of 2.6, the considered variation of soil and masonry stiffness has a relatively small
 322 effect on the LTSM total strain prediction. The total strain is again significantly smaller than the greenfield predictions
 323 because the predicted horizontal strain is essentially zero due to its very low modification factor, combined with the
 324 sagging modification factor. In general, the total strain predictions are most sensitive to uncertainties in the trough
 325 width parameter. This is because changing the trough width significantly affects the LTSM strain, which subsequently
 326 affects all RSM predictions. Consistently with previous observations, the structure exhibits increasing tensile strains
 327 for increasing values of volume loss (plots not shown).

328 3.6.6. Total effective sensitivity index

329 As described in Section 3.5, the sensitivity of the model to the analysed parameters (Table 7) was quantified by
 330 the total effective sensitivity index S_{Ti} (Figures 16 and 17). Since $\sum_{i=1}^P S_{Ti} \geq 1$, the indices were normalised as

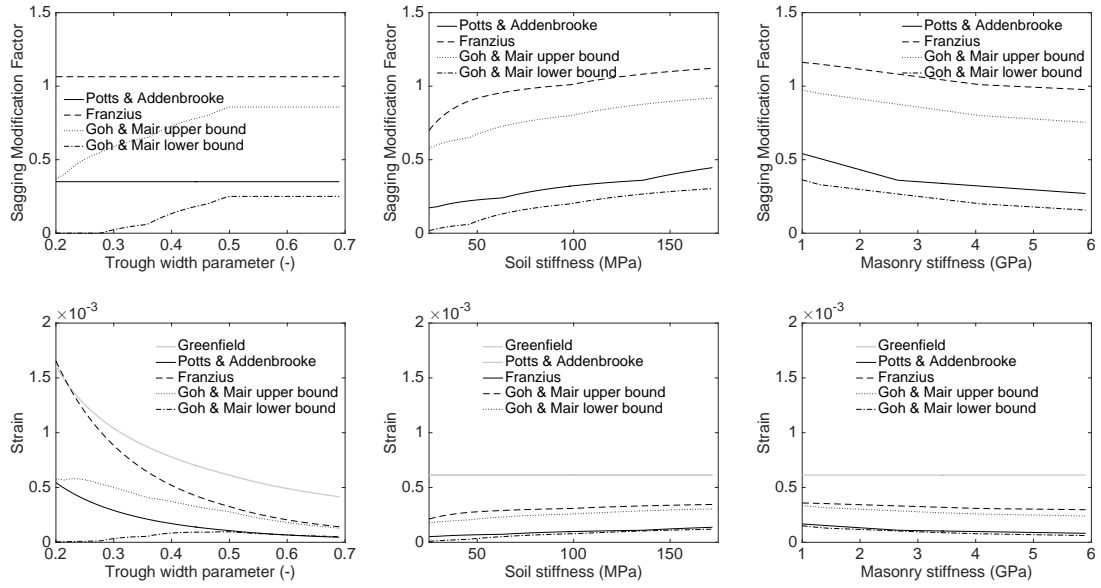


Figure 15: Sensitivity study results, modification factors vs uncertain material parameters.

331 $S_{Ti,n} = \frac{S_{Ti}}{\sum_{i=1}^P S_{Ti}}$. The relationship between input and output variations was evaluated both in terms of modification
 332 factors and strain values for all the considered RSMs.

333 For the tunnel and building parameters (Figure 16), the global sensitivity analysis was used to generalise the
 334 observed trends to the entire space of input variations, removing the potential dependency from the reference building
 335 parameters. Figures 16a and 16b confirm the different variability of the different RSMs, and Figure 16c validates the
 336 appropriateness of the governing factor selection. As expected, the modification factors exhibit a high sensitivity to
 337 the structural parameters (e.g. the building height, since the building stiffness depends on H^3), while the variation

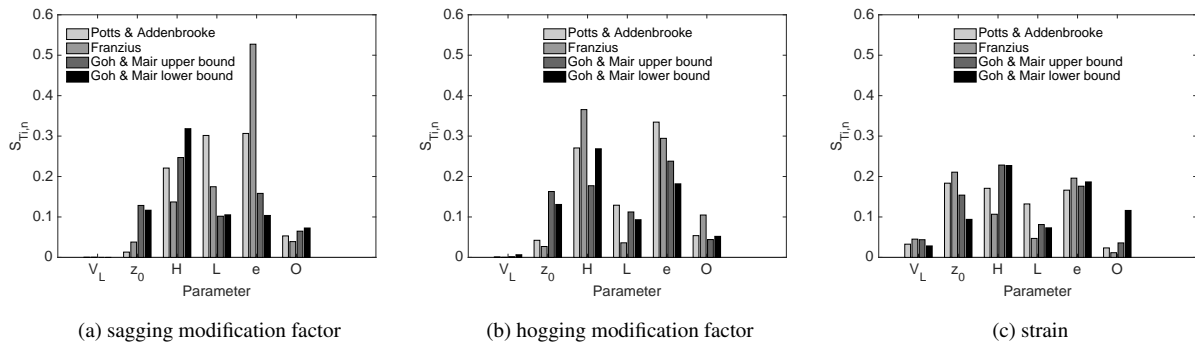


Figure 16: Total effective sensitivity index for tunnel and building geometrical parameters.

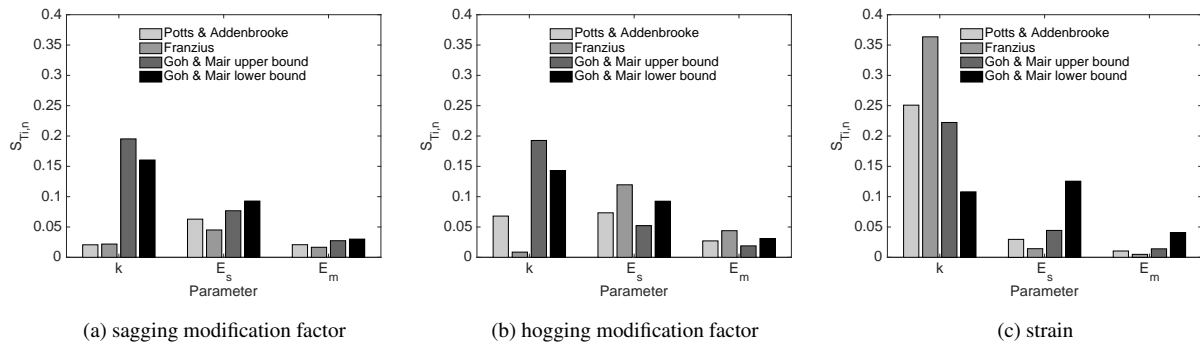


Figure 17: Total effective sensitivity index for material parameters.

338 of volume loss has a negligible effect, since it impacts the greenfield and structure-affected settlement profile in a
 339 proportional way. The strains are subjected to a generally more equal dependency on the input parameters, e.g.
 340 confirming the relatively high impact of the tunnel depth.

341 Differently from the geometrical parameters, the estimation of building and soil material parameters can be af-
 342 fected by a relatively high level of uncertainties. The global analysis was therefore used in this case to quantify the
 343 effect of parameter uncertainties on the output variations. Figure 17 confirms the previously observed trends with re-
 344 spect to the modification factors and strain values, e.g. highlighting the generally larger effect of k on the final strains,
 345 if compared to the effect of soil and masonry stiffness variation.

346 4. Case study

347 In this section the relative stiffness method is applied to a case study from the London Underground Jubilee
 348 Line Extension. The aim is to evaluate the influence of (a) the structural assumptions and uncertainties in the building
 349 stiffness calculation and (b) the different formulations of the method on the final damage assessment of a real structure.
 350 The selected building is the Neptune House at Moodkee Street (Figure 18). This is a 3-storey load bearing masonry
 351 building affected by the construction of the two Jubilee Line tunnels and not subjected to any preliminary protective
 352 measure. The building, dated 1931, is approximately 40 m by 8 m in plan and has concrete strip footings [17]. Figure
 353 19 shows the location of the 5 m diameter twin tunnels that are 17 m deep and were excavated in 1996 (first the
 354 Westbound –WB– tunnel and then the Eastbound –EB– 5 months later).

355 For twin tunnels, the location of the inflection point for the combined settlement trough induced by the two tunnels
 356 depends on the distance between the two tunnel axes. Assuming that the volume loss, the tunnel depth and the trough
 357 width parameter are similar for both tunnels, three general scenarios can be expected (Fig. 20, Crossrail [24]).

358 The Neptune House was mainly affected by the EB tunnel excavation. The two long façades, east and west,
 359 inclined at a 61 degree angle with respect to the EB tunnel axis, were subjected to a hogging deformation from the



Figure 18: Neptune House, view from the North West [23].

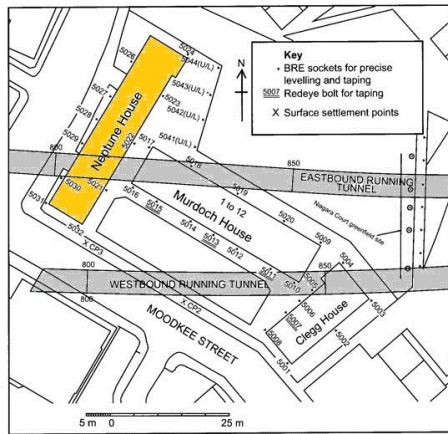


Figure 19: Plan of Neptune House and JLE running tunnels (after Mair and Taylor [17]).

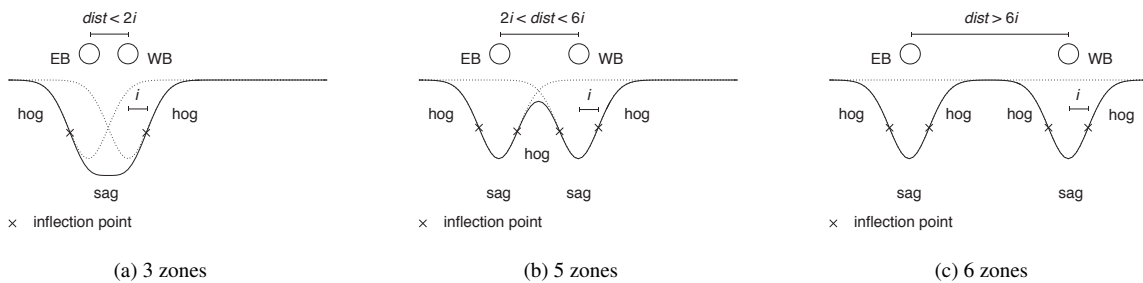


Figure 20: General trough shapes for twin tunnels (after [24]). The number of sagging (sag) and hogging (hog) zones depends on the distance ($dist$) between the Eastbound (EB) and the Westbound (WB) tunnel and on the distance (i) between each inflection point and the corresponding tunnel.

360 WB tunnel and to a combination of hogging and sagging deformations from the EB tunnel. Table 8 reports the
 361 observed deformation parameters [25].

Table 8: Deformation parameters for the Neptune House [25].

Façade	Angle to tunnel	Max differential	Max Δ_s/L_s	Max Δ_h/L_h
Façade	axis (deg)	settlement (mm)		
West façade – WB	58	2	–	3×10^{-5}
East façade – WB	58	3	–	4×10^{-5}
West façade – EB	61	4	4×10^{-5}	2×10^{-5}
East façade – EB	61	4	7×10^{-5}	3×10^{-5}

362 Mair and Taylor [17] gave an initial estimation of the building damage by assuming that the building response
 363 was governed by the masonry walls. Later, Dimmock and Mair [18] inferred the bending stiffness by the observed
 364 deformation parameters and related modification factors. Since the back calculated stiffness in hogging and sagging
 365 were 1 and 2 orders of magnitude lower than the predicted ones, respectively, Dimmock and Mair [18] reformulated
 366 the estimation by neglecting the contribution of the walls in hogging and by reducing the stiffness by one order of
 367 magnitude because of the windows.

368 This paper analyses in detail the impact of different assumptions related to the following factors:

- 369 • **Façade** The contribution of the façade to the global building stiffness can be either included or neglected.
- 370 • **Openings** The effect of window openings can be either neglected or taken into account by reducing EI by
 371 90%.
- 372 • **Slab** The stiffness contribution of the slab can be either included or neglected.
- 373 • **Foundation** The foundation contribution can be included or neglected.
- 374 • **Neutral axis** The position of the neutral axis can be either assumed at half of the building height or calculated
 375 based on all element contributions to the global stiffness.

376 The different assumption combinations considered in this study are reported in Table 9. Case 2 represents the
 377 reference scenario, where the contribution of the façade is included, the stiffness is reduced by 40% to take the
 378 openings into account, both the ground floor slab and foundation are assumed to contribute to the building stiffness
 379 and the position of the neutral axis was calculated by including all primary structural elements.

380 Figure 21 shows the results in terms of bending stiffness for the east façade. The main contribution to the bending
 381 stiffness comes from the façade and the foundation strips, and can be largely dependent on the neutral axis position.
 382 Assuming the neutral axis at the mid-height of the structure increases the calculated stiffness by 42% (case 1), while
 383 neglecting the façade results in a negligible global stiffness (case 4). Without the façade, the neutral axis moves closer
 384 to the foundation, and therefore the foundation contribution to the bending stiffness is also significantly reduced.

385 Figure 22 shows the modification factors obtained for each of the assumed combinations by applying the RSMs.
 386 The monitored modification factors back-calculated from field monitoring data are 0.3 in sagging and 1 in hogging,

Table 9: Assumed combinations of structural features.

Case	1	2	3	4	5	6
Façade	X	X	X		X	X
Openings	X	X			X	
Slab	X	X	X	X		
Foundation	X	X	X	X		
Neutral axis	1/2 height	calculate	calculate	calculate	calculate	calculate

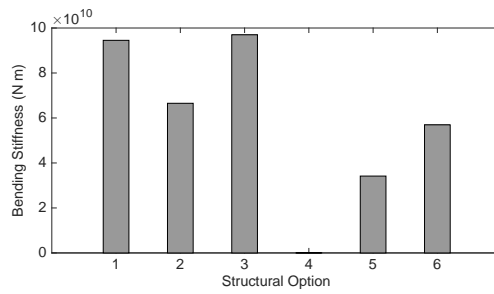


Figure 21: Neptune House case study: building stiffness for assumed combinations.

387 and are also plotted for comparison. As expected, the negligible global stiffness that results from ignoring the façade
388 (case 4) leads to the highest modification factors for all formulations. At the other extreme, including the façade
389 but ignoring openings (case 3), results in the lowest modification factors, both in sagging and in hogging. For the
390 reference case (case 2), Potts and Addenbrooke and Goh & Mair’s upper bound formulations give the best prediction
391 for sagging, while Franzius’ prediction is the closest to reality in the hogging case. Goh & Mair underpredict the
392 response in hogging because the building partition method causes the length in the hogging zone to be relatively
393 short, which predicts an unrealistically rigid structure. Goh & Mair’s upper and lower bounds are the most sensitive to
394 this variation. This sensitivity is mainly connected to the design curves. By increasing the relative bending stiffness,
395 Goh & Mair’s curves lead to a more rapid decrease in modification factors. For the specific sagging case analysed,
396 $\rho_{\text{sag,par}}^*$ is high enough for Goh & Mair’s lower bound to predict that the building is essentially fully rigid ($M^{\text{DR,sag}} \simeq 0$)
397 unless the façade is completely ignored (case 4).

398 In general, the assessment given by Franzius et al. [5] is the most conservative, while the accuracy of the Goh
399 and Mair predictions varied considerably whether the structure was in hogging or sagging, again because of the
400 partitioning method employed. The same analysis has been performed on the west façade and by taking into account
401 the effect of the EB tunnel only. The results do not differ significantly from the ones presented above.

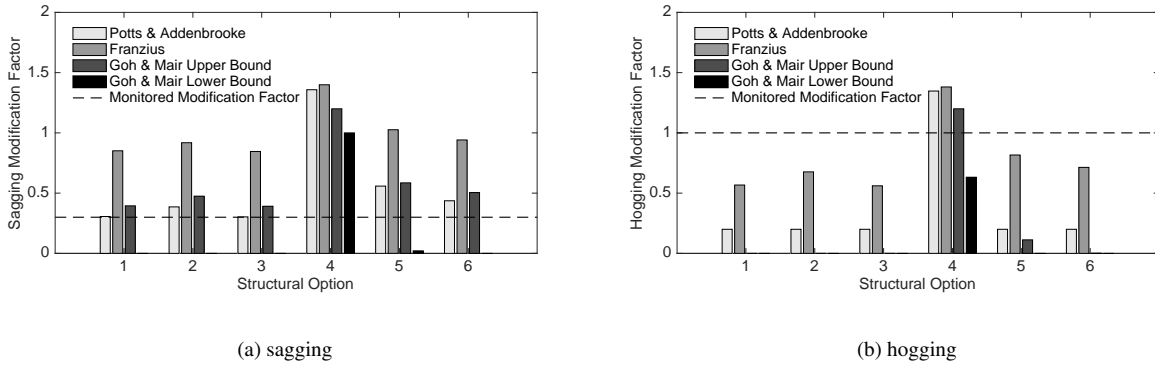


Figure 22: Neptune House case study: modification factors for assumed combinations.

402 5. Conclusions

403 This paper evaluated the available methods for the rapid assessment of settlement-induced damage to surface
 404 structures. In particular, it focused on the different formulations of the relative stiffness method, and on the available
 405 procedures for the calculation of building stiffness.

406 A sensitivity study performed on a number of structures by varying the building height-to-length ratio, eccentricity-
 407 to-trough width ratio, opening ratio, tunnel cover-to-diameter, soil and masonry stiffness, and trough width parameter
 408 made it possible to quantify the influence of these factors on the building stiffness calculation and final damage as-
 409 sessment. Results showed that the original RSM formulation by Potts and Addenbrooke [3] tends to give a prediction
 410 contained between the upper and lower curves by Goh and Mair [6], while the predictions provided by Franzius et al.
 411 [5] tends to be the most conservative.

412 In order to exemplify the actual effect of structural assumptions and different RTM formulations on damage pre-
 413 dictions, these formulations were applied to a masonry building affected by the construction of the Jubilee Line in
 414 London. The results quantified the relative impact of the building façade, of window openings, and of the assumed
 415 neutral axis position on the global building stiffness calculation. Furthermore, they showed that the largest impact on
 416 the final assessment, apart from ignoring the façade entirely, is given by the RSM selection. These results provide
 417 information to guide engineers as they apply these approaches in practice, and information to aid the development of
 418 more robust and consistent procedures in the future.

419 Acknowledgements

420 Financial support was provided by Crossrail and by the Engineering and Physical Sciences Research Council of the
421 United Kingdom, under Grant reference number EP/K018221/1. The research materials supporting this publication
422 can be accessed at <https://doi.org/10.17863/CAM.11563>.

423 References

- 424 [1] G. E. Torp-Petersen, M. G. Black, Geotechnical investigation and assessment of potential building damage arising from ground movements:
425 CrossRail, Proceedings of the Institution of Civil Engineers-Transport 147 (2) (2001) 107–119.
- 426 [2] R. J. Mair, R. N. Taylor, J. B. Burland, Prediction of ground movements and assessment of risk of building damage due to bored tunnelling, in:
427 R. Mair, R. Taylor (Eds.), Geotechnical Aspects of Underground Construction in Soft Ground. Proceedings of the International Symposium,
428 Balkema, Rotterdam, 713–718, 1996.
- 429 [3] D. M. Potts, T. I. Addenbrooke, A structure's influence on tunnelling-induced ground movements, Proceedings of the Institution of Civil
430 Engineers: Geotechnical Engineering 125 (2) (1997) 109–125.
- 431 [4] M. Son, E. J. Cording, Estimation of building damage due to excavation-induced ground movements, Journal of Geotechnical and Geoenvironmental
432 Engineering 131 (2) (2005) 162–177.
- 433 [5] J. N. Franzius, D. M. Potts, J. B. Burland, The response of surface structures to tunnel construction, Proc Inst Civil Eng: Geotech Eng 159 (1)
434 (2006) 3–17.
- 435 [6] K. H. Goh, R. J. Mair, The response of buildings to movements induced by deep excavations, Geotechnical Engineering Journal of the SEAGS
436 and AGSSEA 42 (3).
- 437 [7] J. B. Burland, B. B. Broms, V. F. B. de Mello, Behaviour of foundations and structures, in: Proc. 9th Int. Conf. Soil Mech. and Found. Eng.,
438 vol. 2, 495–546, 1977.
- 439 [8] M. D. Boscardin, E. J. Cording, Building response to excavation-induced settlement, Journal of Geotechnical Engineering 115 (1) (1989)
440 1–21.
- 441 [9] S. Timoshenko, Strength of materials: Elementary theory and problems, 1, D. Van Nostrand, 3rd edn., 1957.
- 442 [10] J. B. Burland, C. P. Wroth, Settlement of buildings and associated damage, in: Proceedings of Conference on Settlement of Structures,
443 Pentech Press, Cambridge, 611–654, 1974.
- 444 [11] H. D. Netzel, Building response due to ground movements, Ph.D. thesis, Delft University of Technology, 2009.
- 445 [12] J. B. Burland, J. R. Standing, F. M. Jardine, Building response to tunnelling: case studies from construction of the Jubilee Line Extension,
446 London, CIRIA Special Publication Series, Thomas Telford, London, 2001.
- 447 [13] J. B. Burland, R. J. Mair, R. N. Standing, Ground performance and building response due to tunnelling, in: R. J. Jardine, D. M. Potts, K. G.
448 Higgins (Eds.), Conference on Advances in Geotechnical Engineering, vol. 1, Institution of Civil Engineers, 291–342, 2004.
- 449 [14] R. J. Mair, Tunnelling and deep excavations: ground movements and their effects, in: A. e. a. Anagnostopoulos (Ed.), Proceedings of the
450 15th European Conference on Soil Mechanics and Geotechnical Engineering - Geotechnics of Hard Soils - Weak Rocks (Part 4), IOS Press,
451 39–70, 2013.
- 452 [15] G. G. Meyerhof, Some recent foundation research and its application to design, The Structural Engineer 31 (1953) 151–167.
- 453 [16] M. Melis, J. Rodriguez Ortiz, Consideration of the stiffness of buildings in the estimation of subsidence damage by EPB tunnelling in the
454 Madrid subway, in: Response of Buildings to Excavation Induced Ground Movements Conference, London, 2001.
- 455 [17] R. J. Mair, R. N. Taylor, vol. 1, chap. Settlement predictions for Neptune, Murdoch and Clegg Houses and adjacent masonry walls, CIRIA
456 special publication 200, London, 217–228, 2001.
- 457 [18] P. S. Dimmock, R. J. Mair, Effect of building stiffness on tunnelling-induced ground movement, Tunnelling and Underground Space Technol-
458 ogy 23 (2008) 438–450.

- 459 [19] R. Peck, Deep excavations and tunneling in soft ground, in: Proceedings of the 7th International Conference on Soil Mechanics and Founda-
460 tion Engineering, Mexico City, 225–290, 1969.
- 461 [20] M. O'Reilly, B. New, Settlement above tunnels in the United Kingdom – their magnitude and prediction, in: Tunnelling 82. Proceedings of
462 the 3rd International Symposium, Institution of Mining and Metallurgy, London, 173–181, 1982.
- 463 [21] T. Homma, A. Saltelli, Importance measures in global sensitivity analysis of nonlinear models, Reliability Engineering & System Safety 52
464 (1996) 1–17, ISSN 09518320, doi:10.1016/0951-8320(96)00002-6, URL [http://www.sciencedirect.com/science/article/pii/
465 0951832096000026](http://www.sciencedirect.com/science/article/pii/0951832096000026).
- 466 [22] S. Miro, D. Hartmann, T. Schanz, Global sensitivity analysis for subsoil parameter estimation in mechanized tunneling, Computers and
467 Geotechnics 56 (2014) 80–88, ISSN 0266352X, doi:10.1016/j.compgeo.2013.11.003, URL [http://dx.doi.org/10.1016/j.compgeo.
468 2013.11.003](http://dx.doi.org/10.1016/j.compgeo.2013.11.003).
- 469 [23] J. A. Pickhaver, H. J. Burd, G. T. Housby, An equivalent beam method to model masonry buildings in 3D finite element analysis, Computers
470 & Structures 88 (19-20) (2010) 1049–1063.
- 471 [24] Crossrail, Phase 2 Generic Building Damage Assessment Report – Drive X Running Tunnels, Tech. Rep., 2011.
- 472 [25] P. Dimmock, Tunnelling-induced ground and building movement on the Jubilee Line Extension, Ph.D. thesis, University of Cambridge, 2003.